The Meteoritical Society

Meteoritics & Planetary Science 42, Nr 2, 171–184 (2007)
Abstract available online at http://meteoritics.org

Petrology of the Miller Range 03346 nakhlite in comparison with the Yamato-000593 nakhlite

N. IMAE[1, 2*] and Y. IKEDA[3]

[1]Antarctic Meteorite Research Center, National Institute of Polar Research,
The Graduate University for Advanced Studies, Kaga 1-chome, Itabashi-ku, Tokyo 173-8515, Japan
[2]Department of Polar Science, School of Multidisciplinary Science,
The Graduate University for Advanced Studies, Kaga 1-chome, Itabashi-ku, Tokyo 173-8515, Japan
[3]Department of Material and Biological Sciences, Ibaraki University, Mito 310-8512, Japan
*Corresponding author. E-mail: imae@nipr.ac.jp

(Received 23 June 2006; revision accepted 22 November 2006)

Abstract–We petrologically examined the Miller Range (MIL) 03346 nakhlite. The main-phase modal abundances are 67.7 vol% augite, 0.8 vol% olivine, and 31.5 vol% mesostasis. Among all known nakhlites, MIL 03346's modal abundance of olivine is the smallest and of mesostasis is the largest. Augite occurs as cumulus phenocrysts having a homogeneous core composition ($En_{36–38}Fs_{24–22}Wo_{40}$), which is identical with other nakhlites. They accompany thin ferroan rims divided into inner and outer rims with a compositional gap at the boundary between the two rims. Olivine grains have magnesian cores (Fa ≥ 55) and show normal zoning toward ferroan rims (Fa ≤ 84). Mesostasis consists mostly of glass (26.0 vol%) with minor skeletal fayalites, skeletal titanomagnetites, acicular phosphate, massive cristobalite, and sulfides. We conclude that MIL 03346 is the most rapidly cooled nakhlite among all known nakhlites based on the petrography.

We obtain the intercumulus melt composition for MIL 03346 from the mass balance calculation using the modal abundances and discuss the crystallization sequence of MIL 03346 in comparison with that of Yamato (Y-) 000593. Although magnesian olivines of Y-000593 are phenocrystic, magnesian olivine grains of MIL 03346 seem to have texturally crystallized from the intercumulus melt. After the MIL 03346 magma intruded upward to the Martian surficial zone, the magnesian olivine crystallized, and then the ferroan inner rim formed on phenocrystic core augite. The outer rim of phenocrystic augites formed after the crystallization of skeletal fayalites and skeletal titanomagnetites, resulting in a compositional gap between the inner and outer rims. Finally, glassy mesostasis formed from the residual melt. This crystallization sequence of MIL 03346 is different from those of other nakhlites, including Y-000593.

INTRODUCTION

The recent recovery of many meteorites from Antarctica and hot deserts has greatly increased the number of recognized Martian meteorites (e.g., Meyer 2004). The number of recognized nakhlites has also increased; as of May 2006, seven independent nakhlites have been recognized. The total weight of all nakhlites is ~30 kg.

Nakhlites are igneous cumulates consisting of main phenocrystic augites, minor olivines, titanomagnetites, and siliceous mesostasis (e.g., Treiman 2005). Their crystallization and ejection ages are 1.3 Gyr and 10–12 Myr, respectively (Okazaki et al. 2003). Petrological studies of nakhlites have been focused on magmatic petrogenesis (Harvey and McSween 1992; Treiman 1993; Imae et al. 2005). Secondary alteration of nakhlites has formed clays and evaporites in minor amounts on fractures and margins in olivine grains (Gooding et al. 1991; Treiman et al. 1993; Treiman and Lindstrom 1997; Bridges and Grady 2000; Bridges et al. 2001). Recent progress of the nakhlite studies is reviewed in detail by Treiman (2005).

Several differences among nakhlites have been recognized by studies of new nakhlites: the differences are in bulk chemical compositions, chemical zoning of phenocrystic olivines (Mikouchi et al. 2000, 2005a), modal abundances of constituent phases, thickness of phenocrystic augite rims (Imae and Ikeda 2006), crystallinity of the groundmass, and degree of aqueous alteration (Bridges and Grady 2000;

Grady et al. 2005). The bulk composition of Miller Range (MIL) 03346 is somewhat poorer in Mg and Fe and is richer in Na, K, and Al than those of other nakhlites (Anand et al. 2005). The groundmass of MIL 03346 is characteristically glassy in comparison to other nakhlites.

Although petrographic studies have been carried out (Mikouchi et al. 2005b; McKay and Schwandt 2005; Anand et al. 2005; Day et al. 2006), we present the petrology of MIL 03346 in detail and compare it with the Yamato (Y-) 000593 nakhlite, including the paired two specimens of Y-000749 and Y-000802. We obtained the intercumulus melt compositions from the mass balance calculation using the bulk compositions and the modal mineral abundances for the both nakhlites. We clarified the crystallization sequence by which the two rims of augites and the mesostasis of MIL 03346 formed, and show the difference in the crystallization sequence between the MIL 03346 and Y-000593 nakhlites.

ANALYTICAL METHODS

The polished thin section used for this study was MIL 03346,8 (Fig. 1a), with a surface area of 66 mm^2. The modal abundances of the constituent minerals in MIL 03346,8 were determined by weighing each area extracted from enlarged photographs using a microbalance. An electron-probe microanalyzer (EPMA) (JEOL JXA-8200) at the National Institute of Polar Research was used for the chemical analyses of minerals and glass. The beam current was 11 nA with a focused beam for minerals, and 3 nA with a defocused beam of 10 μm for glass to prevent the alkali loss. Apparent bulk compositions of magmatic inclusions were determined from modal abundances of glass, minerals, and ferroan augite halos in the inclusions. The Bence and Albee's correction method was used for silicates and oxides, and the ZAF method was used for sulfides.

The Raman spectra for silica minerals in the MIL 03346 and Y-000593 nakhlites were obtained on polished thin sections of MIL 03346,8 and Y-000749,1-1 using a JASCO NRS-1000 Raman microspectrometer at the National Institute of Polar Research. A focused green laser beam with a wavelength of 531.91 nm and an intensity of 11 mW was used for the analyses.

The mass balance calculation to estimate the melt compositions for the MIL 03346 and Y-000593 nakhlites was carried out by the method of Imae et al. (2005).

PETROLOGY OF THE MIL 03346 NAKHLITE

The MIL 03346 nakhlite has a cumulative texture and consists mainly of phenocrystic augites and mesostasis with minor magnesian olivine grains (Fig. 1a). Modal abundances of the constituent phases are 67.7 vol% phenocrystic augite, 0.8 vol% magnesian olivine, and 31.5 vol% mesostasis. The MIL 03346 nakhlite was described by Day et al. (2006), Mikouchi et al. (2005b), McKay and Schwandt (2005), and several other groups presenting at the 36th Lunar and Planetary Science Conference in 2005. In this paper, we expand on the existing description.

Phenocrystic Augites

The grain sizes of phenocrystic augites are smaller than 1 × 0.5 mm (Figs. 1a and 1b), and the average area of phenocrystic augites is 0.12 mm^2. Polysynthetic twinnings are common in phenocrystic augites. The phenocrystic augites consist of cores and rims, and the modal abundance of augites (67.7 vol%) is divided into two portions: 56.5 vol% for cores and 11.2 vol% for rims. The core augites have a nearly homogeneous composition of $En_{36–38}Fs_{24–22}Wo_{40}$ (Fig. 2; Table 1), which is consistent with those by Day et al. (2006) and others. The rims are ferroan (Table 1) and have a thickness of ~20 μm on average. The Al_2O_3 content of the rims increases up to 10 wt%, and the TiO_2 content also increases up to 1.5 wt% (Fig. 3). The boundaries between the cores and rims are straight and distinctive in backscattered electron images (Fig. 1c). The ferroan rims develop on the side facing the mesostasis, but not on the boundary with augite or olivine grains.

The ferroan rims are divided into inner and outer rims toward the boundary with mesostasis (Figs. 2 and 3). There is a compositional gap between the inner and outer rims (Fig. 3), and the boundary between them is clear under an optical microscope and in a backscattered electron image (Fig. 1c). The Fe# [= Fe/(Fe + Mg)] of both rims increases outward (Fig. 2). Wo contents of the inner rim slightly decrease outward, and those of the outer rim slightly increase outward (Fig. 3). The Al_2O_3 contents of rims continue to increase outward through both rims (Fig. 3). The outer rims sometimes contain small titanomagnetite grains several micrometers in size (Fig. 1c), whose composition is similar to skeletal titanomagnetites in mesostasis. Therefore the titanomagnetite grains in the mesostasis may co-crystallize with the outer rims, and the crystallization of titanomagnetites suppresses the increase of the TiO_2 content in the outer rim (Fig. 3).

Magnesian Olivine Grains

Magnesian olivine grains rarely occur in MIL 03346 and the number of magnesian olivine grains in our polished thin section is only three. The modal abundance of magnesian olivine in MIL 03346 (0.8 vol%) is much lower than in the Y-000593 nakhlite (10 vol%) and other nakhlites (e.g., 10.8 vol% for Nakhla and 12.5 vol% for NWA 817) (Treiman 2005). The grain sizes are smaller than 0.5 × 0.5 mm (Fig. 1b). The occurrence of the magnesian olivine grains suggests that they may have crystallized from an interstitial melt between cumulus augites (Fig. 1b). Although some large olivine grains a few millimeters in size are contained in other

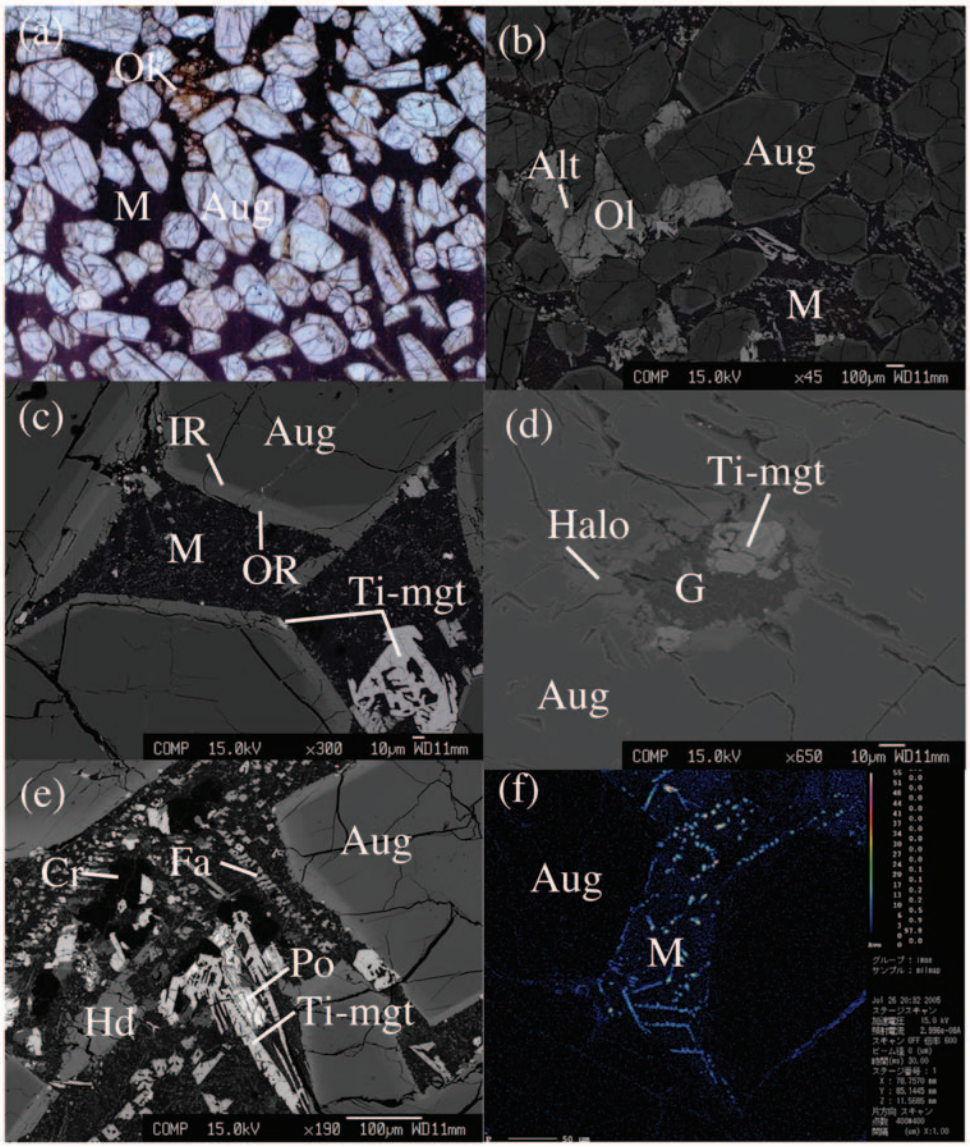

Fig. 1. a) A polished thin section of MIL 03346,8 under an optical microscope. The width is 5 mm. b) Backscattered electron image of MIL 03346,8 with a low magnification. The scale bar is 100 μm. c) Mesostasis and augite phenocryst rims under the backscattered electron image. Rim is divided into the inner rim (IR) and the outer rim (OR). The scale bar is 100 μm. d) A magmatic inclusion in an augite phenocryst core under the backscattered electron image. The scale bar is 100 μm. e) Enlarged mesostasis under the backscattered electron image. f) A concentration map of phosphorus in mesostasis. The concentration of calcium in the phosphorus rich area in mesostasis has a positive correlation with the concentration of phosphorus. Electron beam current = 30 nA. The scale bar at the bottom is 50 μm. Aug = augite. Ol = olivine, M = mesostasis, Ti-mgt = titanomagnetite, IR = the inner rim on a phenocryst augite core, OR = the outer rim on a phenocryst augite core, Halo = ferroan augite halo, G = glassy phase, Cr = cristobalite, Hd = hedenbergite, Alt = hydrous-altered phase, and Po = pyrrhotite.

thin sections, they are also interstitial to phenocrystic augites (e.g., Day et al. 2006). The compositions of the olivine cores are magnesian ($Fa_{55–57}$), and they show normal zoning to ferroan rims (up to Fa_{84}) (Fig. 4; Table 1). The CaO content of the magnesian olivines is in the range of 0.4–0.6 wt% (Fig. 4). Skeletal fayalites occur in mesostasis, and have more ferroan composition than those of the olivine rims (Fig. 1e). They seem to have overgrown rapidly from the mesostasis melt.

The magnesian olivine grains sometimes accompany weathered rims or weathered fractures (Fig. 1b), where two types of secondary altered phases are recognized. In the backscattered electron image they are lighter and darker phases, corresponding to the ferroan phase (probably serpentine) and silica-rich phase (probably saponite), respectively (Table 1).

Mesostasis

A glassy phase is the most abundant (26.0 vol%) in mesostasis (Figs. 1c and 1e), and the simply averaged composition of 79 points, obtained by the broad beam of an EPMA 10 μm in diameter, is shown in Table 1. In more

Table 1. Representative compositions of constituent minerals and glassy phase in MIL 03346 (wt%).

Phase	Augite	Augite	Hedenbergite	Ferroan pyroxene	Hedenbergitic pyroxene	Ferroan augite	Olivine grain	Olivine grain	Olivine grain	Skeletal fayalite
Occurrence	Phenocrystic core average (n = 218)	Phenocrystic inner rim	Phenocrystic outer rim	Mesostasis	Mesostasis	Halo in inclusion (#4) in phenocryst augite (n = 8)	Core	Rim	Rim (dendritic portion)	Mesostasis
SiO_2	52.05	48.25	44.05	47.45	48.04	47.00	34.00	32.56	31.70	30.47
TiO_2	0.27	0.46	2.52	0.86	0.78	0.94	0.03	0.04	0.04	0.11
Al_2O_3	0.96	2.48	6.74	3.37	0.90	4.69	0.07	0.00	0.05	0.06
FeO	14.04	27.66	24.64	27.34	29.81	23.98	45.36	55.54	60.34	63.07
MnO	0.41	0.75	0.41	0.66	0.84	0.61	0.95	1.14	1.67	2.02
MgO	12.66	6.32	2.54	5.04	1.23	4.17	19.39	10.55	6.54	2.71
CaO	19.13	13.91	19.49	15.51	18.52	16.94	0.51	0.56	0.42	0.20
Na_2O	0.28	0.28	0.45	0.28	0.25	0.63	0.00	0.00	0.00	0.00
K_2O	0.01	0.00	0.01	0.01	0.00	0.08	0.01	0.00	0.00	0.02
P_2O_5	0.02	0.01	0.02	0.04	0.02	0.11	0.04	0.00	0.08	0.11
Cr_2O_3	0.22	0.00	0.02	0.00	0.00	0.01	0.02	0.00	0.02	0.00
Total	100.04	100.13	100.89	100.56	100.38	99.28	100.36	100.39	100.86	98.75
En	36.91	19.86	8.35	15.98	3.93	14.03	–	–	–	–
Fs	22.98	48.73	45.52	48.66	53.49	45.16	–	–	–	–
Wo	40.12	31.40	46.12	35.36	42.58	40.81	–	–	–	–
Fa	–	–	–	–	–	–	56.75	74.71	83.81	92.89

Phase	Cristobalite	Titanomagnetite	Glassy phase	Glassy phase	Serpentine	Saponite		Pyrrhotite	Chalcopyrite
Occurrence	Mesostasis	Mesostasis	Mesostasis (n = 79) 10 μm beam	Inclusion (#4) in phenocryst augite (n = 3) 10 μm beam	Fracture in olivine grain	Fracture in olivine grain		Mesostasis	Mesostasis
SiO_2	98.43	0.16	59.40	58.62	32.36	46.78	S	39.38	35.41
TiO_2	0.08	7.71	0.56	0.29	0.05	0.03	Fe	59.98	32.37
Al_2O_3	1.10	0.96	17.81	19.88	0.09	2.26	Co	0.03	0.11
FeO	0.36	83.76	7.94	6.68	55.53	30.57	Ni	0.04	0.04
MnO	0.00	0.34	0.09	0.04	1.27	0.52	Cu	0.00	32.70
MgO	0.01	0.05	0.19	0.13	5.75	3.57	Total	99.42	100.62
CaO	0.12	0.11	4.38	3.96	0.13	0.21			
Na_2O	0.10	0.00	5.84	6.19	0.03	0.07			
K_2O	0.01	0.01	1.17	2.06	0.00	0.09			
P_2O_5	0.00	0.02	1.14	0.62	0.00	0.01			
Cr_2O_3	0.00	0.00	0.02	0.01	0.00	0.00			
SO_3	–	–	0.63	0.37	–	–			
NiO	–	–	0.04	0.04	–	–			
Total	100.20	93.12	99.22	98.90	95.21	84.10			

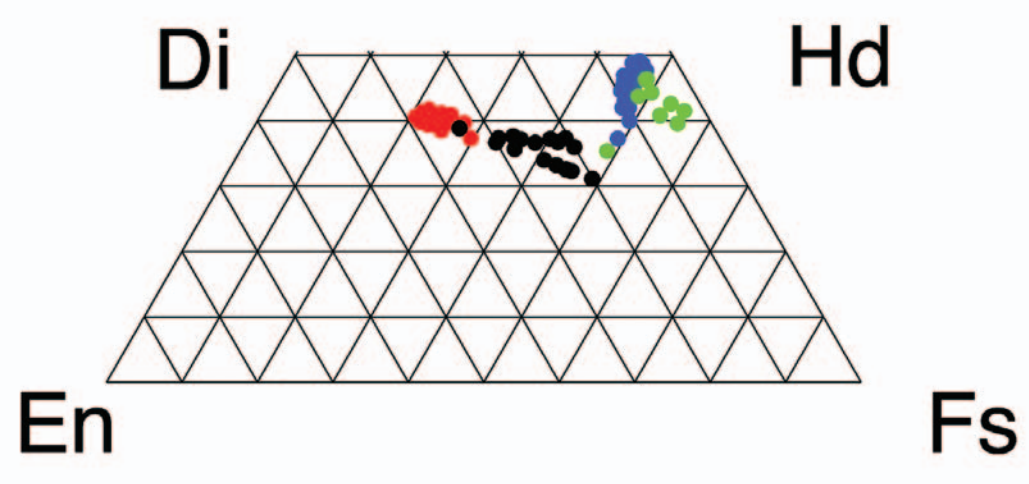

Fig. 2. The composition of pyroxenes as a plot of the wollastonite-enstatite-ferrosilite ternary system. There is a compositional gap between the inner rim augites and the outer rims. Red circles = core augite compositions, black circles = the inner rim augite compositions, blue circles = the outer rim hedenbergites, and green circles = hedenbergites in mesostasis.

detail, Day et al. (2006) classified glass in mesostasis into four types (Al-rich, Al-poor, Si-rich, and K- and P-rich), and they showed that glass is dominated by the Al-rich one in trachy-andesite field classified in the SiO_2-(Na_2O + K_2O) diagram. Our data are also mostly in the field. No plagioclases are found in mesostasis, but skeletal fayalites ($Fa_{92–95}$; 3.3 vol%) (Table 1; Fig. 1e) and skeletal titanomagnetites (2.2 vol%) (Table 1; Fig. 1e) are abundant there. The CaO content of the skeletal fayalites is 0.15–0.2 wt%, which is lower than that of magnesian olivine grains (Fig. 4). The skeletal fayalites are several tens of micrometers in length and ~10 μm in width. Skeletal titanomagnetites always accompany thin ilmenite lamellae of ~0.2 μm, and are similar in composition to those included in the outer rims of phenocrystic augites. Tiny acicular phosphates (probably apatite) (Fig. 1f) (McKay and Schwandt 2005) and a massive silica mineral (cristobalite) (Fig. 5) (Chennaoui Aoudjehane et al. 2006) of ~100 μm in size (Fig. 1e) commonly occur in mesostasis. Sulfides several micrometers in size are found in mesostasis, and consist of mostly pyrrhotites ($Fe_{0.85–0.89}S$) (Fig. 1e; Table 1), sometimes coexisting with minor chalcopyrite. The pyroxene in mesostasis is hedenbergitic, and the compositions are more ferroan than those of the outer rims of phenocrystic augite (Table 1; Fig. 2).

DISCUSSION: COMPARISON OF MIL 03346 WITH Y-000593

The Y-000593 nakhlite is a typical nakhlite, similar in lithology to the previously known Nakhla and Governador Valadares (Mikouchi et al. 2003; Imae et al. 2003, 2005; Treiman 2005). However, MIL 03346 has many features that are different from Y-000593. Therefore, we compare MIL 03346 with Y-000593 in the following discussion.

Bulk Compositions

The whole rock composition of MIL 03346 (Anand et al. 2005) is different from that of Y-000593 (Imae et al. 2003). The former is richer in Al_2O_3, Na_2O, and K_2O, and poorer in MgO and FeO + Fe_2O_3 than the latter (Table 2), although the SiO_2 and CaO contents are nearly the same between them.

The difference in whole rock composition corresponds mainly to the difference in modal abundance of mesostasis (32 vol% for MIL 03346 and 10 vol% for the Y-000593 nakhlite). The composition of mesostasis is also different between the two: the mesostasis of MIL 03346 is olivine-normative, but that of Y-000593 is silica-normative. As modal abundance of magnesian olivines in MIL 03346 (0.8 vol%) is much less than in Y-000593 (about 10 vol%; Imae et al. 2003), the lower contents of MgO and FeO of the MIL 03346 whole rock seem to reflect the lower modal olivine in MIL 03346.

Constituent Minerals

Grain sizes of phenocrystic augites in MIL 03346 are slightly smaller than those in Y-000593: the averages of phenocrystic augites are 0.32 mm^2 for Y-000593 and 0.12 mm^2 for MIL 03346. The En, Fs, and Wo contents of phenocrystic core augites for MIL 03346 are nearly the same as those for Y-000593 (Table 1) (Imae et al. 2005). However, subtle irregular compositional variations of Al, Ti, and Cr contents in a single phenocrystic core augite have been recognized for several nakhlites (McKay and Mikouchi 2005; McKay et al. 2006).

The augite rims in MIL 03346 (Fig. 1c) are thinner than those in Y-000593 (Imae et al. 2003, 2005), and the modal abundance of augite rims for MIL 03346 (11.2 vol%) is also smaller than that of Y-000593 (15.9 vol%) (Imae et al. 2005). Although the augite inner rims in MIL 03346 are similar in

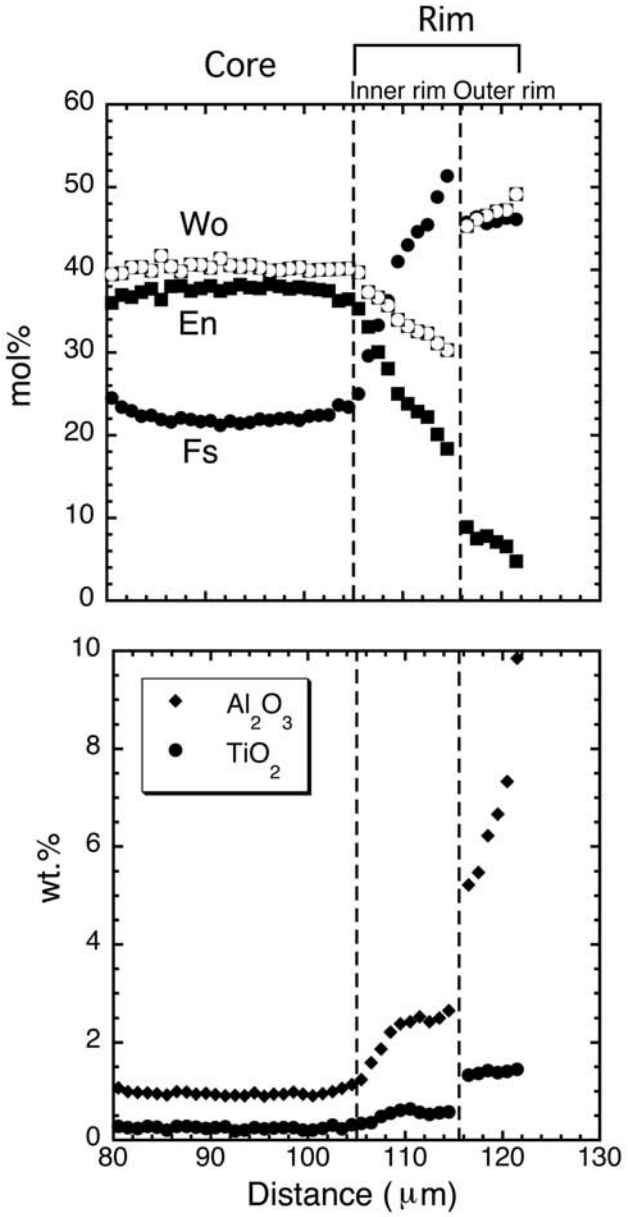

Fig. 3. The chemical zoning of an augite phenocryst contacting with mesostasis. There is a compositional gap between the inner and the outer rims.

composition to those in Y-000593, the outer rims in MIL 03346 are different from those in Y-000593. The outer rims in Y-000593 are continuous in compositions from the inner rims (Fig. 3 in Imae et al. 2005), but a compositional gap at the boundaries is clear between the inner and outer rims of MIL 03346.

Cooling experiments at ~4 °C/h at 1 bar under the condition of the QFM buffer using interstitial melt compositions for nakhlites formed compositional trends of pyroxenes identical to those of phenocrystic augites in MIL 03346 (Imae and Ikeda 2006). These run products show a compositional gap between the ferroan pyroxene and the hedenbergitic rim, indicating that dendritic fayalitic olivines and dendritic titanomagnetites crystallized in mesostasis during the compositional gap (Imae and Ikeda 2006). The experimental evidence shows that the formation of the compositional gap in MIL 03346 is due to the rapid crystallization of the mesostasis minerals between the two rims.

The Al_2O_3 contents of the high Ca pyroxene rims in MIL 03346 (up to 10 wt%) are different from those in Y-000593 (up to 3 wt%). The crystallization of the outer rim with decreasing Al and Ca contents for Y-000593 was subsequent to the crystallization of plagioclase in mesostasis (Imae et al. 2005). However, the high contents of Al_2O_3 in the rims for MIL 03346 may be caused by the suppression of plagioclase crystallization in mesostasis melts. The straight boundaries between cores and rims of phenocrystic augites in MIL 03346 are clear in the backscattered electron image, while the irregular boundaries between core and rim of phenocrystic augites are common in Y-000593 (Fig. 1b in Imae et al. 2005). The irregular core-rim boundaries in Y-000593 can be caused by the adcumulus growth of core augites on a floor of a magma chamber (Wager et al. 1960), but the adcumulus growth was probably negligible for MIL 03346.

Magmatic inclusions in phenocrystic augites are found in both the MIL 03346 and Y-000593 nakhlites (Imae et al. 2005). The number of magmatic inclusions in MIL 03346 is much smaller than in Y-000593. Mineral assemblages of magmatic inclusions are glass, ferroan halo augite, and titanomagnetites, and they are similar to each other in the two nakhlites. However, the glass portion is larger and the ferroan halo augite is thinner in MIL 03346 than in Y-000593. There are no magmatic inclusions or monocrystalline inclusions in olivines of MIL 03346, although olivine in Y-000593 contains magmatic inclusions (Imae et al. 2005).

The most magnesian olivine in MIL 03346 is Fa_{55} (Fig. 4), which is one of the most magnesian among all nakhlites (Fa_{58} for Y-000593), although the olivine rims in MIL 03346 (up to Fa_{84}) are somewhat higher than those in Y-000593 (up to ~Fa_{80}) (Fig. 4; Table 1). The texture of the olivine grain in Fig. 1b shows that the magnesian olivine must have crystallized from the intercumulus melt before the crystallization of the inner rim of phenocrystic augites. Wider compositional zoning of olivine grains in MIL 03346 than in Y-000593 suggests that MIL 03346 cooled more rapidly than Y-000593.

Symplectites and lamellae are not observed in olivine grains or on the boundaries of olivine grains of MIL 03346, although they are common in Y-000593 (Imae et al. 2003; Mikouchi et al. 2003). The formation of symplectites and lamellae may depend on the oxygen fugacity during the crystallization of core olivines and cooling rates of the olivine grains, suggesting they have different cooling histories (Putnis and McConnell 1980).

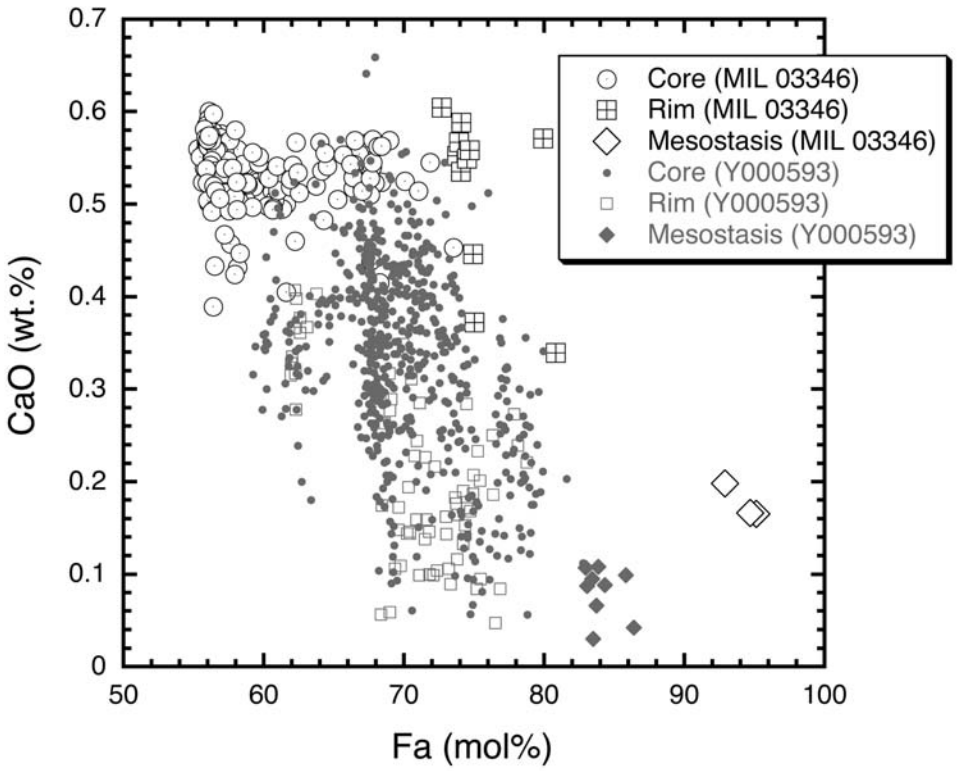

Fig. 4. The CaO contents of olivines plotted against their fayalite (Fa) components. Skeletal fayalites in mesostasis have low CaO contents. Olivine compositions in Y-000593, Y-000749, and Y-000802 are also plotted for reference.

The mesostasis in MIL 03346 is characterized by an abundant glassy phase with minor skeletal fayalite and skeletal titanomagnetites, as is also described by Day et al. (2006), while the mesostasis in Y-000593 is characterized by abundant plagioclase. The skeletal textures of titanomagnetites in mesostasis of MIL 03346 (Fig. 1e) are similar to those in the NWA 817 nakhlite (Sautter et al. 2002), and their occurrence suggests that these nakhlites cooled rapidly. On the other hand, titanomagnetites in Y-000593 occur as microphenocrysts (Imae et al. 2003, 2005), suggesting they have slower cooling. The thickness of ilmenite lamellae exsolved in titanomagnetites is about 0.2 μm for MIL 03346 and is much thinner for Y-000593 (2–3 μm in width). The silica mineral in MIL 03346 is solely cristobalite (Fig. 5) (Chennaoui et al. 2006), while in the Yamato nakhlites, silica minerals are tridymite and cristobalite (Fig. 5) (Imae et al. 2003).

Mass Balance Calculation to Estimate the Intercumulus Melt Composition

The occurrence of olivine grains in MIL 03346 shows that the magnesian olivine is a noncumulus phase (Figs. 1a and 1b). Therefore, the intercumulus melt composition of MIL 03346 is estimated by subtraction of core augite (56.5 vol%) from the major element whole rock composition (Anand et al. 2005). As the TiO_2 content (0.07 wt%) (Table 2) is too low to carry out the mass balance calculation, the TiO_2 content is neglected in the calculation. The obtained intercumulus melt composition for MIL 03346 (MIM) is shown in Table 2. The calculated Fe/Mg partition coefficient between core augite and the intercumulus melt is 0.21 [$=(FeO/MgO)_{core\text{-}augite}/(FeO/MgO)_{MIM}$] (Tables 1 and 2), and this is consistent with the reference data of 0.22 between core augite and the intercumulus melt (Grove and Bence 1977).

Silica, MgO, FeO, and alkali contents of the intercumulus melt for MIL 03346 are similar to those for Y-000593 (Table 2). However, the intercumulus melt in MIL 03346 is richer in alumina and poorer in CaO than the intercumulus melt of Y-000593 (Imae et al. 2005).

Trapped Melt Composition Estimated from Magmatic Inclusions in Phenocrystic Augites

Magmatic inclusions occur within core augites in MIL 03346. We selected larger five magmatic inclusions ~100 μm in size (Fig. 1d). On average, these magmatic inclusions consist of 48.7 vol% glassy phase, 42.5 vol% thin ferroan augite halo, 6.4 vol% titanomagnetite, and 2.4 vol% fayalite. A hydrous phase (saponite) coexisting with fayalitic olivine was observed only in one magmatic inclusion, suggesting that

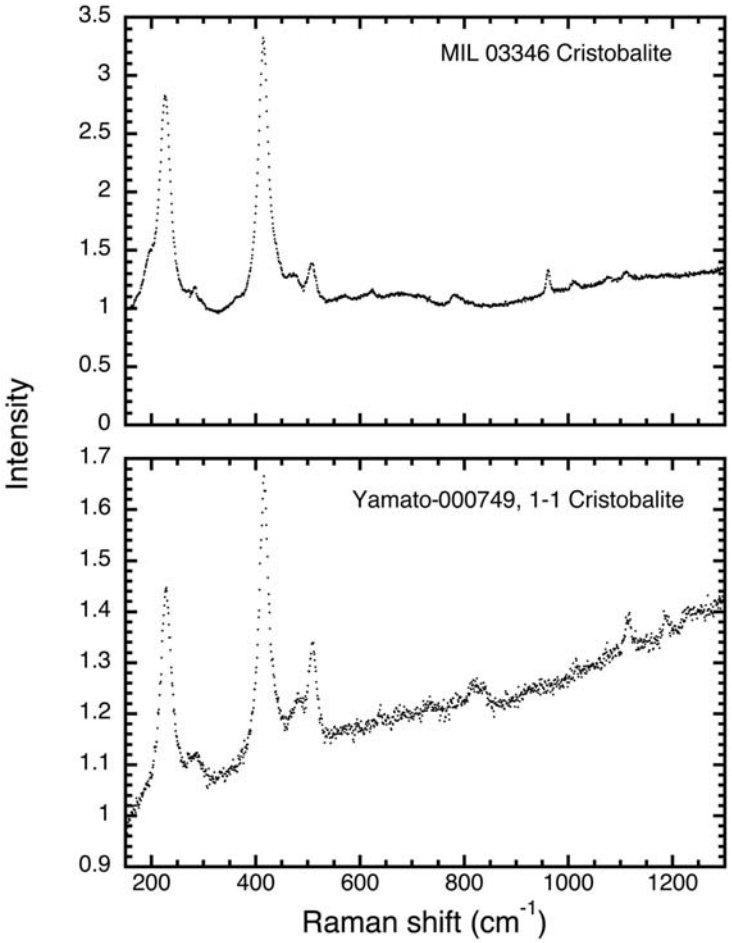

Fig. 5. The Raman spectra for cristobalites in mesostasis in the MIL 03346 and Y-000749 nakhlites.

the phase may have formed by the hydrous alteration of fayalitic olivine on Mars. The average bulk composition of the magmatic inclusion was estimated, the mode of the hydrous phase being included into fayalitic olivine. The chemical compositions of the constituent minerals are shown in Table 1. The apparent composition of the average bulk for five magmatic inclusions is given in Table 2.

We corrected the apparent composition of magmatic inclusions in MIL 03346 (Table 2) through the addition of a wall augite composition identical to phenocrystic core augite to satisfy the Fe/Mg partition between the phenocrystic core augite and the trapped melt composition. The result of the corrections means that the mixing ratio of the magmatic inclusion and wall augite is 79.1 vol% and 20.9 vol%, respectively (Table 2). The corrected trapped melt composition, shown in Table 2, is similar to the intercumulus melt obtained from the mass balance calculation (Table 2) for MIL 03346, except for low FeO and high K_2O and Cr_2O_3 contents for the trapped melt. The compositional difference of the trapped melt with the interstitial melt may be due partly to the restricted number of inclusions, and partly to uncertainty of modal compositions of minerals in magmatic inclusions.

The average composition of magmatic inclusions in phenocrystic core augites of Y-000593 (Table 2) is similar to the estimated trapped melt composition (Table 2) for MIL 03346, although the rapid cooling of MIL 03346 might have formed the larger glass and thinner halo augite within magmatic inclusions than those in Y-000593.

The Crystallization of the Intercumulus Melts in the MIL 03346 and Y-000593 Nakhlites

Based on the texture of MIL 03346 and the crystallization experiments (Imae and Ikeda 2006), the sequence of minerals crystallizing from the intercumulus melt for MIL 03346 is, in order: magnesian olivine, inner-rim augites, skeletal fayalites and titanomagentites, and outer-rim hedenbergite. Final residual melt formed the mesostasis glass. We calculated the residual melts (L1–L5) by sequential subtraction of minerals crystallizing from the interstitial melt, where phosphate, silica, and hedenbergite in the mesostasis

Table 2. Bulk compositions of mesostasis, the intercumulus melt, the magmatic inclusion, and the whole rock of the MIL 03346 nakhlite in comparison with those of the Y-000593 nakhlite.

	MIL 03346 nakhlite					Y-000593 nakhlite			
	Mesostasis[a]	Interstitial melt (MIM)[b]	Apparent inclusion[c]	Corrected trapped melt[d]	Whole rock[e]	Mesostasis[f]	Interstitial melt (YIM)[g]	Trapped melt[h]	Whole rock[i]
SiO_2	50.18	47.02	47.45 (9.6)	48.43	49.20	60.52	47.93	47.10	48.35
TiO_2	2.35	–	2.20 (4.2)	1.79	0.07	0.49	0.16	1.93	0.47
Al_2O_3	14.25	7.27	9.95 (3.0)	8.03	3.59	15.68	5.05	6.69	1.96
FeO*	22.16	26.90	24.38 (11.8)	22.17	19.23	9.69	26.44	24.15	21.55
MnO	0.33	0.52	0.47 (0.2)	0.46	0.45	0.18	0.81	0.44	0.59
MgO	0.40	5.14	2.15 (1.2)	4.40	9.33	0.95	4.95	5.82	11.09
CaO	3.44	9.92	8.78 (5.6)	11.00	15.00	3.96	11.42	11.35	14.90
Na_2O	4.53	2.03	2.25 (1.4)	1.83	1.01	5.10	1.82	1.83	0.66
K_2O	0.91	0.68	1.48 (1.5)	1.16	0.29	2.12	0.58	0.30	0.17
P_2O_5	0.91	0.50	0.56 (0.4)	0.44	0.22	0.88	0.65	0.24	0.21
Cr_2O_3	0.02	0.01	0.04 (0.04)	0.08	0.13	0.01	0.19	0.15	0.26
SO_3	0.49	–	0.24 (0.3)	0.19	–	–	–	–	0.08[j]
NiO	0.03	–	0.06 (0.08)	0.05	0.06	–	–	–	–
Total	100.00	99.99	100.01	100.03	98.58	99.58	100.00	100.00	100.21

[a]Bulk composition of mesostasis consisting of glassy phase, skeletal fayalites, skeletal titanomagnetites, acicular phosphate, massive cristobalite, and sulfides.
[b]Interstitial melt composition for MIL 03346 (MIM). According to Dyar et al. (2005), FeO* = 26.90 wt% is divided into FeO = 21.04 wt% and Fe_2O_3 = 5.90 wt%.
[c]Averaged apparent composition from five magmatic inclusions in augites in MIL 03346. The parentheses are 2σ.
[d]Corrected composition of magmatic inclusion.
[e]Whole-rock composition of MIL 03346 by Anand et al. (2005). According to Dyar et al. (2005), FeO* = 19.23 is divided into FeO = 15.05 wt% and Fe_2O_3 = 4.2 wt%.
[f]Bulk composition of mesostasis of Y-000749 analyzed in the present study under the 50 μm diameter electron beam (n = 39). Mesostasis consists of main plagioclase and minor K-feldspar, cristobalite, tridymite, titanomagnetite, pigeonite, apatite, ferroan olivine, and pyrrhotite.
[g]Interstitial melt composition of the Y-000593 nakhlite (YIM) recalculated Fe_2O_3 as FeO. Cumulus olivine = 7.82 vol%. Intercumulus olivine = 4.38 vol%.
[h]Averaged 4 sets of magmatic inclusions consisting of glass, titanomagnetite, and ferroan halo in phenocryst core augites in Y-000749.
[i]Whole-rock composition of the Y-000593 nakhlite (Imae et al. 2003). FeO* is divided into FeO = 19.51 wt% and Fe_2O_3 = 2.04 wt%.
[j]Concentration as FeS.
FeO* = FeO + Fe_2O_3.

Table 3. The modal abundances of main constituent phases for the MIL 03346 and Y-000593 nakhlites.

Augite	Olivine	Mesostasis	References
MIL 03346			
0.74	0.04	0.22	Mikouchi et al. (2005b)
0.798	0.046	0.157	McKay and Schwandt (2005)
0.65	0	0.35	Rutherford et al. (2005)
0.78	0.02	0.19	Stopar et al. (2005)
>0.70	–	–	Kinman and Neal (2005)
~0.70	–	~0.25	Anand et al. (2005)
0.677	0.008	0.315	This study
Y-000593			
0.767	0.122	0.111	Imae et al. (2005)
0.8	0.1	0.1	Mikouchi et al. (2003)

are not included because of their negligible modal abundances.

The modal abundances of magnesian olivine and mesostasis differ among different sections of MIL 03346. The abundances range from 0–4.6 vol% for magnesian olivine and 15.7–35 vol% for mesostasis (Anand et al. 2005; Kinman and Neal 2005; McKay and Schwandt 2005; Mikouchi et al. 2005b; Rutherford et al. 2005; Stopar et al. 2005; this study) (Table 3). Therefore, we assumed a set of modal abundance of minerals crystallizing from the intercumulus melt to obtain a residual melt having the mesostasis glass in MIL 03346 (Fig. 6; Table 4). The assumed modal abundances are 3.9 vol% magnesian olivine, 11.2 vol% inner-rim augite, 2.2 vol% fayalite, 1.3 vol% titanomagnetite, and 8.7 vol% outer-rim hedenbergite (Fig. 6). Residual melts are calculated using the abundances of minerals and plotted in Fig. 6. The final residual melt (L5) for this case is plotted near the mesostasis glass.

The sequence of minerals crystallizing from the intercumulus melt for Y-000593 is, in order: overgrowth olivine surrounding cumulus olivines, inner-rim augites, and outer-rim pyroxenes (Imae et al. 2005). The final residual melt crystallized plagioclase, K-feldspar, apatite, pyrrhotite, ferroan olivine, pigeonite, titanomagnetite, cristobalite, and tridymite in the mesostasis (Imae et al. 2003, 2005).

The magma of the Y-000593 nakhlite included cumulus olivine (Fa_{50}) of 8 vol% in equilibrium with phenocrystic core augite (Imae et al. 2005), and cooled more slowly than that of MIL 03346. The obtained original intercumulus melt for Y-000593 (YIM) is shown in Table 5 (Imae et al. 2005). As the cumulus magnesian olivine became ferroan (about Fa_{65}) during the slow cooling of the interstitial melt, we estimated the melt (L1) with the diffusional modification of cumulus olivine composition. The residual melts (L2–L3) were calculated using the measured modal abundance of minerals crystallizing from the intercumulus melt for Y-000593 (Table 5). L1 is the melt after the crystallization of overgrowth olivine of Fa_{65} (3 vol%), which is the averaged composition of phenocrystic olivines ($Fa_{60–75}$) in Y-000593, L2 after the crystallization of the inner rim augites (15 vol%), L3 after the crystallization of the outer rim pyroxenes (1 vol%) (Table 5). We plotted the intercumulus melt composition and the residual melt compositions in Harker's variation diagrams (Fig. 6). The calculated residual melt composition after the growth of the outer rim pyroxene (L3) coincides roughly with the mesostasis in the figures.

In Fig. 7, we schematically present the crystallization sequence that formed MIL 03346. Phenocrystic core augites in MIL 03346 accumulated in a magma chamber. After the upward intrusion, magnesian olivine grains started to crystallize from the intercumulus melt. The inner rim augites surrounding phenocrystic core augites may have formed in a lava flow or in a chilled margin of a sill under rapid cooling conditions. The crystallization of skeletal fayalites and skeletal titanomagnetites resulted in a compositional gap between inner and outer rims. The outer rims and acicular hedenbergite crystals in the mesostasis crystallized with cristobalite, sulfides, and phosphate in the latest stage of crystallization. Finally, the residual melt was quenched as glass.

Cooling Histories for Nakhlites

Nakhlites seem to have formed under various cooling rates in lava flows or sills that were caused by eruption or upward intrusion of magmas. The bulk compositions of nakhlites and the modal abundances of core augites are very similar among all nakhlites. On the other hand, modal amounts and chemical zoning of phenocrystic olivines, rims of phenocrystic augites, and mineral assemblages in mesostasis are different among nakhlites. These differences may correspond to different cooling rates among nakhlites.

MIL 03346 cooled more rapidly than all other nakhlites, and the rate is several degrees Celsius per hour, based on the crystallization experiments of intercumulus melts (Imae and Ikeda 2006). On the other hand, Y-000593 cooled moderately (about 0.1–1 °C/h), and Nakhla, Govenador Valadares, and Lafayette may have cooled more slowly (<0.1 °C/h) (Mikouchi and Miyamoto 2002; Imae et al. 2003). Recently, Grady et al. (2005) proposed the chilled margin model with

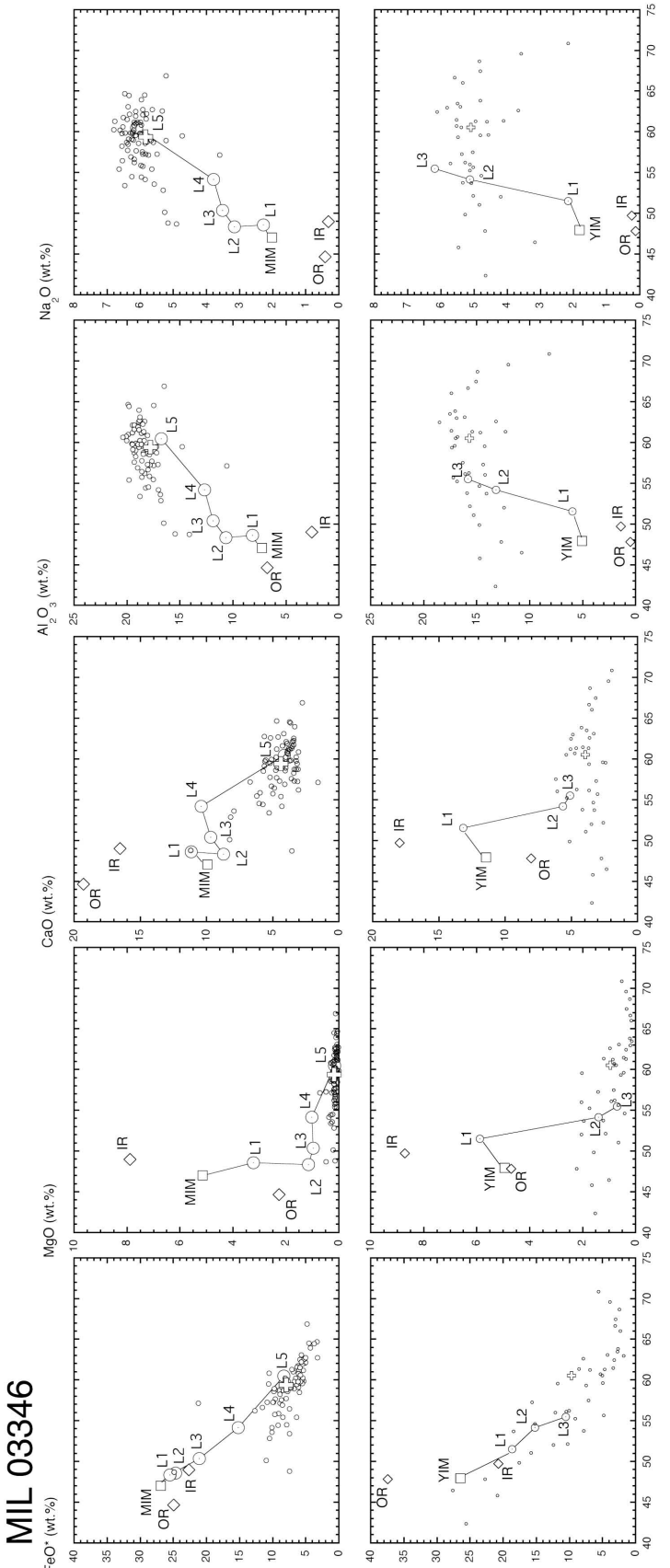

Fig. 6. Harker's variation diagrams of FeO* (=FeO + Fe_2O_3), MgO, CaO, Al_2O_3, and Na_2O versus SiO_2 showing the residual melt trends from the intercumulus melts (MIM and YIM). The upper five diagrams are for MIL 03346, and lower five diagrams are for the Yamato nakhlites. L1–L5 of MIL 03346 is listed in Table 3, and L5 is similar to mesostasis glass. L1–L3 of Y-000593 is listed in Table 5, and L3 is within compositions of mesostasis. Open cross = averaged glassy mesostasis composition for MIL 03346, and averaged mesostasis composition for Y-000593. Small open circles = raw data of glassy mesostasis for MIL 03346 and mesostasis for Y-000593, IR = inner rim surrounding phenocrystic augites, OR = outer rim surrounding phenocrystic augites.

Table 4. The compositional change (L1–L5) of melt by the crystallization of the intercumulus melt for MIL 03346 toward mesostasis glass.

	MIM	Fa_{55}	L1	Inner rim	L2	Fa_{93}	L3	Ti-mgt	L4	Outer rim	L5
SiO_2	47.02	34.25	48.59	48.98	48.33	30.47	50.37	0.16	54.16	44.64	60.45
TiO_2	–	0.00	–	0.63	–	0.11	–	7.71	–	1.78	–
Al_2O_3	7.27	0.00	8.16	2.57	10.65	0.06	11.88	0.96	12.70	6.75	16.77
Cr_2O_3	0.01	0.00	0.01	0.03	0.00	0.00	0.00	0.00	0.00	0.01	0.00
FeO	26.90	45.06	24.68	22.68	25.53	63.07	21.06	83.76	15.23	24.97	8.31
MnO	0.52	0.00	0.58	0.60	0.58	2.02	0.40	0.34	0.40	0.54	0.31
MgO	5.14	20.69	3.24	7.89	1.15	2.71	0.96	0.05	1.03	2.26	0.16
CaO	9.92	0.00	11.14	16.54	8.70	0.20	9.69	0.11	10.41	19.28	4.13
Na_2O	2.03	0.00	2.28	0.32	3.15	0.00	3.52	0.00	3.79	0.42	6.11
K_2O	0.68	0.00	0.76	0.01	1.10	0.02	1.23	0.01	1.32	0.02	2.22
P_2O_5	0.50	0.00	0.56	0.01	0.81	0.11	0.89	0.02	0.95	0.10	1.54
Total	99.99	100.00	100.00	100.26	100.00	98.77	100.00	93.12	100.00	100.77	100.00
Density	3.30	4.00	3.23	3.50	3.12	4.30	3.03	5.00	2.92	3.50	2.61
Mode	0.44	0.04	0.40	0.11	0.29	0.02	0.27	0.01	0.25	0.09	0.17
Normalized mode	1.00	0.09	0.91	0.26	0.65	0.05	0.60	0.03	0.57	0.20	0.37

Table 5. The compositional change (L1–L3) of melt by the crystallization of the intercumulus melt for the Y-000593 nakhlite toward bulk mesostasis based on Imae et al. (2005).

	YIM	Fa_{65}	L1	Inner rim	L2	Outer rim	L3
SiO_2	47.93	31.78	51.53	49.70	54.16	47.82	55.48
TiO_2	0.16	0.00	0.19	0.35	–	0.30	–
Al_2O_3	5.05	0.00	5.99	1.38	13.16	0.51	15.84
Cr_2O_3	0.19	0.03	0.22	0.10	0.41	0.03	0.49
FeO	26.44	49.48	18.64	20.76	15.25	37.45	10.52
MnO	0.81	1.00	0.77	0.51	1.18	1.08	1.21
MgO	4.95	14.94	5.87	8.72	1.40	4.70	0.69
CaO	11.42	2.00	13.17	17.97	5.63	8.03	5.11
Na_2O	1.82	0.00	2.16	0.25	5.13	0.13	6.19
K_2O	0.58	0.00	0.69	0.01	1.74	0.00	2.11
P_2O_5	0.65	0.00	0.77	0.02	1.94	0.00	2.35
NiO	–	0.00	–	0.02	–	0.00	–
Total	100.00	100.00	100.00	99.79	100.00	100.05	99.99
Density	3.08	4.12	2.92	3.41	2.38	3.71	2.21
Mode	0.30	0.03	0.27	0.14	0.12	0.01	0.11
Normalized mode	1.00	0.11	0.89	0.47	0.43	0.05	0.38

deep burial depth as for the geological setting of MIL 03346 to explain the mineral assemblages of secondary altered phases.

CONCLUSIONS

1. Higher alumina and alkalis contents of the whole rock composition for MIL 03346 correspond to the higher modal abundance of mesostasis than other nakhlites.
2. There is a line of evidence that the intercumulus melt for MIL 03346 cooled more rapidly than that of Y-000593: glassy mesostasis, thinner halo augite and massive glass in magmatic inclusions within phenocrystic augites, more magnesian olivine grains in the core, and hedenbergitic outer rim surrounding phenocrystic augites.
3. The crystallization sequence of MIL 03346 is as follows: cumulus minerals of core augites crystallized to form crystal mush at the bottom of a magma chamber. The crystal mush intruded upward and magnesian olivine grains crystallized from the intercumulus melt in lava flow or the chilled margin in a sill. Subsequently, the inner and outer rims of phenocrystic augite crystallized. Between the formation of inner and outer rims, skeletal fayalites and skeletal titanomagnetites formed in mesostasis, resulting in the compositional gap between inner and outer rims. Finally, mesostasis glass formed.

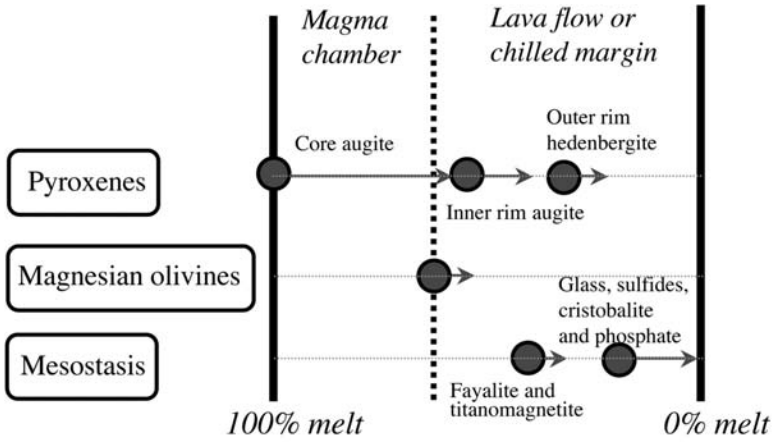

Fig. 7. This schematic illustration shows the plausible crystallization sequence of constituent phases from the magma chamber toward lava flow or sill for MIL 03346.

4. The interstitial melt composition of MIL 03346 seems to be slightly different from that of Y-000593; the alumina content is higher and the CaO content is lower for MIL 03346.

Acknowledgments–We are grateful to NASA JSC for lending us the polished thin section for this study. We are also grateful to Dr. Treiman for his handling of our manuscript and to Drs. Mikouchi and Calvin for their constructive reviews. This research is partly supported by JSPS, Grant-in-Aid for Scientific Research (15540463) and by NIPR, Research Project Funds, P8 (Evolution of the Early Solar System Materials).

Editorial Handling—Dr. Allan Treiman

REFERENCES

Anand M., Williams C. T., Russell S. S., Jones G., James S., and Grady M. M. 2005. Petrology and geochemistry of nakhlite MIL 03346: A new Martian meteorite from Antarctica (abstract #1639). 36th Lunar and Planetary Science Conference. CD-ROM.

Bridges J. C. and Grady M. M. 2000. Evaporite mineral assemblages in the nakhlite (Martian) meteorites. *Earth and Planetary Science Letters* 176:267–279.

Bridges J. C., Catling D. C., Saxton J. M., Swindle T. D., Lyon I. C., and Grady M. M. 2001. Alteration assemblages in Martian meteorites: Implications for near-surface processes. *Space Science Reviews* 96:365–392.

Chennaoui A. H., Jambon A., and Boudouma O. 2006. Cristobalite and K-feldspar in the nakhlite MIL 03346: A cathodoluminescence study (abstract #1037). 37th Lunar and Planetary Science Conference. CD-ROM.

Day J. M. D., Taylor L. A., Floss C., and McSween H. Y., Jr. 2006. Petrology and chemistry of MIL 03346 and its significance in understanding the petrogenesis of nakhlites on Mars. *Meteoritics & Planetary Science* 41:581–606.

Dyar M. D., Treiman A. H., Pieters C. M., Hiroi T., Lane M. D., and O'Connor V. 2005. MIL 03346, the most oxidized Martian meteorite: A first look at spectroscopy, petrography, and mineral chemistry. *Journal of Geophysical Research* 110, doi:10.1029/2005JE002426.

Gooding J. L., Wentworth S. J., and Zolensky M. E. 1991. Aqueous alteration of the Nakhla meteorite. *Meteoritics* 26: 135–143.

Grady M. M., Anand M., Bridges J., Pearson V., Verchovsky A. B., and Franchi I. A. 2005. Aqueous alteration of nakhlites: Results from Y-000593 and MIL 03346, and implications for water on Mars (abstract). 29th Symposium on Antarctic Meteorites. pp. 17–18.

Grove T. L. and Bence A. E. 1977. Experimental study of pyroxene-liquid interaction in quartz-normative basalt 15597. Proceedings, 8th Lunar Science Conference. pp. 1549–1579.

Harvey R. P. and McSween H. Y., Jr. 1992. The parent magma of the nakhlite meteorite: Clues from melt inclusions. *Earth and Planetary Science Letters* 111:467–482.

Imae N., Ikeda Y., Shinoda K., Kojima H., and Iwata N. 2003. Yamato nakhlites: Petrography and mineralogy. *Antarctic Meteorite Research* 16:13–33.

Imae N., Ikeda Y., and Kojima H. 2005. Petrology of the Yamato nakhlites. *Meteoritics & Planetary Science* 40:1581–1598.

Imae N. and Ikeda Y. 2006. Crystallization of nakhlite melts in comparison with synthetic experiments (abstract). 30th Symposium on Antarctic Meteorites. pp. 35–36.

Irving A. J., Kuehner S. M., Rumble D. III, Carlson R. W., and Hupé G. M. 2002. Petrology and isotopic composition of orthopyroxene-bearing nakhlite NWA 998 (abstract). *Meteoritics & Planetary Science* 37:A70.

Kinman W. S. and Neal C. R. 2005. Petrology of nakhlite MIL 03346 (abstract #1660). 36th Lunar and Planetary Science Conference. CD-ROM.

McKay G. and Schwandt C. 2005. Mineralogy and petrology of new Antarctic nakhlite MIL 03346 (abstract #2351). 36th Lunar and Planetary Science Conference. CD-ROM.

McKay G. and Mikouchi T. 2005. Minor element zoning in nakhlites: What's going on? (abstract). *Meteoritics & Planetary Science* 40: A100.

McKay G., Schwandt C., Le L., Makishima J., Mikouchi T., and Kurihara T. 2006. Minor elements in nakhlite pyroxenes: Cr in MIL 03346 (abstract). 30th Symposium on Antarctic Meteorites. pp. 59–60.

Meyer C. 2004. Mars Meteorite Compendium. http://www-curator.jsc.nasa.gov/curator/antmet/mmc/mmc.htm.

Mikouchi T., Yamada I., and Miyamoto M. 2000. Symplectic

exsolution in olivine from the Nakhla Martian meteorite. *Meteoritics & Planetary Science* 35:937–942.

Mikouchi T. and Miyamoto M. 2002. Comparative cooling rates of nakhlites as inferred from iron-magnesium and calcium zoning of olivines (abstract #1343). 33rd Lunar and Planetary Science. CD-ROM.

Mikouchi T., Koizumi E., Ueda Y., Miyamoto M., and McKay G. 2005a. On the relationship between mineralogical characteristics and relative burial depths of nakhlites (abstract). 29th Symposium on Antarctic Meteorites. pp. 41–42.

Mikouchi T., Monkawa A., Koizumi E., Chokai J., and Miyamoto M. 2005b. MIL 03346 nakhlite and NWA 2737 ("DIDEROT") chassignite: Two new Martian cumulate rocks from hot and cold deserts (abstract #1944). 36th Lunar and Planetary Science Conference. CD-ROM.

Okazaki R., Nagao K., Imae N., and Kojima H. 2003. Noble gas signatures of Antarctic nakhlites, Yamato (Y-) 000593, Y-000749, and Y-000802. *Antarctic Meteorite Research* 16:58–79.

Putnis A. and McConnell J. D. C. 1980. *Principles of mineral behaviour*. Oxford: Blackwell Scientific Publications. 257 p.

Rutherford M. J., Calvin C., Nicholiss M., and McCanta M. 2005. Petrology and melt compositions in nakhlite MIL 03346: Significance of data from natural sample and from experimentally fused groundmass and M.I.'s (abstract #2233). 36th Lunar and Planetary Science Conference. CD-ROM.

Sautter V., Barrat J. A., Jambon A., Lorand J. P., Gillet P., Javoy M., Joron J. L., and Lesourd M. 2002. A new Martian meteorite from Morocco: The nakhlite Northwest Africa 817. *Earth and Planetary Science Letters* 195:223–238.

Stopar J. D., Lawrence S. J., Lentz R. C. F., and Taylor G. J. 2005. Preliminary analysis of nakhlite MIL 03346, with a focus on secondary alteration (abstract #1547). 36th Lunar and Planetary Science Conference. CD-ROM.

Treiman A. H. 1993. The parent magma of the Nakhla (SNC) meteorite, inferred from magmatic inclusions. *Geochimica et Cosmochimica Acta* 57:4753–4767.

Treiman A. H., Barrett R. A., and Gooding J. L. 1993. Preterrestrial aqueous alteration of the Lafayette (SNC) meteorite. *Meteoritics* 28:86–97.

Treiman A. H. and Lindstrom D. J. 1997. Trace element geochemistry of Martian iddingsite in the Lafayette meteorite. *Journal of Geophysical Research* 102:9153–9163.

Treiman A. H. 2005. The nakhlite meteorites: Augite-rich igneous rocks from Mars. *Chemie der Erde* 65:203–270.

Wager L. R., Brown G. M., and Wadsworth W. J. 1960. Types of igneous cumulates. *Journal of Petrology* 1:73–85.